ERJ open research
THE BEST IN OPEN ACCESS BASIC, TRANSLATIONAL & CLINICAL RESPIRATORY RESEARCH

Early View

Original article

Anti-HSP47 siRNA Lipid Nanoparticle ND-L02-s0201 Reverses Interstitial Pulmonary Fibrosis in Preclinical Rat Models

Yun Liu, Jian Liu, Alistair Quimbo, Fengcheng Xia, Jiping Yao, Jean-Pierre Clamme, Sonya Zabludoff, Jun Zhang, Wenbin Ying

Please cite this article as: Liu Y, Liu J, Quimbo A, *et al*. Anti-HSP47 siRNA Lipid Nanoparticle ND-L02-s0201 Reverses Interstitial Pulmonary Fibrosis in Preclinical Rat Models. *ERJ Open Res* 2021; in press (https://doi.org/10.1183/23120541.00733-2020).

Anti-HSP47 siRNA Lipid Nanoparticle ND-L02-s0201 Reverses Interstitial Pulmonary Fibrosis in Preclinical Rat Models

Yun Liu[†], Jian Liu[†], Alistair Quimbo, Fengcheng Xia, Jiping Yao, Jean-Pierre Clamme, Sonya Zabludoff, Jun Zhang[‡], Wenbin Ying[*]

Affiliations:

Nitto Biopharma Inc. 10618 Science Center Drive, San Diego, CA 92121, USA

[‡] Cellagen Technology, 5940 Pacific Mesa Court, Suite 206, San Diego, CA 92121, USA

[†] These authors had equal contributions to this project

[*] To whom correspondence should be addressed: wenbin.ying@nitto.com

Summary

By targeting production of procollagen chaperone HSP47, which is necessary for the proper folding of procollagen, and by facilitating normalization of epithelial-mesenchymal transition, siRNA lipid nanoparticle ND-L02-s0201 reverses interstitial pulmonary fibrosis, restores structural integrity of the lung and improves pulmonary function in preclinical rat models.

Abstract

ND-L02-s0201 is a lipid nanoparticle encapsulating a siRNA which inhibits expression of heat shock protein 47, a collagen-specific chaperone. Accumulated evidence demonstrates a close association between increased level of HSP47 and excessive

accumulation of collagen in fibrotic diseases. Our objective was to test ND-L02-s0201 efficacy in preclinical lung fibrosis models and characterize the downstream histological and functional consequences of inhibiting the expression of HSP47. Comprehensive optimization and characterization of bleomycin and silica induced rat lung fibrosis models was conducted, which ensured progressive pathological changes were sustained throughout the study during evaluation of the anti-fibrotic potential of ND-L02-s0201. In the bleomycin model, we demonstrated dose-dependent and statistically significant reduction in lung weight, collagen deposition and histology and fibrosis scores following ND-L02-s0201 treatment. Lung tissue mRNA profiling demonstrated that 11 out of 84 fibrosis relevant genes were upregulated following bleomycin induction and further maximally downregulated approximately four-and-half folds after ND-L02-s0201 treatment. Epithelial-mesenchymal transition was characterized in the bleomycin model following ND-L02-s0201 treatment. Cell enrichment demonstrated myofibroblasts contained the highest HSP47 mRNA expression. Bleomycin led to a more than five-fold increase in myofibroblasts and ND-L02-s0201 treatment reduced the myofibroblasts to Sham levels. Statistically significant improvement in lung function was noted in bleomycin model determined by running endurance capacity using a seven-minute treadmill test. Comparable anti-fibrotic efficacy was also observed in the silica model. Results from two robust chronic rodent models of pulmonary fibrosis demonstrated significant anti-fibrotic effects and improved lung function which support the evaluation of ND-L02-s0201 in subjects with idiopathic pulmonary fibrosis.

Introduction

Idiopathic pulmonary fibrosis (IPF) is a specific form of chronic, progressive fibrotic interstitial pneumonia of unknown cause. The prevalence increases with age and the pathological changes are limited to the lungs. IPF is characterized by progressive worsening of dyspnea and lung function and is associated with a poor prognosis [1]. The median survival of idiopathic pulmonary fibrosis patients is generally two to three years after diagnosis. Respiratory failure resulting from disease progression is the most frequent cause of death [2].

Advances have been made in the past decades in understanding the pathogenesis of idiopathic pulmonary fibrosis. Initially IPF was considered as the result of chronic inflammation, but current evidence suggests idiopathic pulmonary fibrosis may be caused by an abnormal wound healing process. Repeated alveolar epithelial cell injury or apoptosis, with abnormal re-epithelialization, continuous fibroblast to myofibroblast transition, and progressive extracellular matrix accumulation, result in lung tissue destruction and fibrosis, eventually leading to respiratory compromise and failure [3] [4]. Myofibroblast as a key cell type have been identified involving in fibrosis progression in response to signals of tissue damage, participating in tissue remodeling and wound repair through the regulated deposition and maintenance of the extracellular matrix (ECM) components [5]. In addition to fibroblast [6] [7], other cell types including bone marrow-derived circulating pluripotent mesenchymal progenitor (fibrocyte) [8] and endothelial [9] have been demonstrated playing important roles in myofibroblast recruitment and enrichment through the epithelial-to-mesenchymal transition (EMT) or endothelial-to-mesenchymal transition (EndMT) mechanisms. The presence of multiple-source recruitment of myofibroblasts, sustained activation,

continuous proliferation and survival results ultimately in impaired tissue repair due to excessive ECM synthesis and deposition.

Heat shock protein 47 (HSP47) is a collagen-specific molecular chaperone residing in the endoplasmic reticulum (ER), which is essential for the correct folding of procollagen in the ER. The expression of HSP47 under normal conditions correlates with collagens in various cell types and tissues, helps maintain hemostasis and the integrity of tissue structure. Additionally, HSP47 has been reported to play a pivotal role in pathological conditions such as fibrotic diseases, which include excessive collagen accumulation and deposition within interstitial space. Elevation of HSP47 expression has been observed in multiple forms of fibrosis [10] [11] [12]. Preclinical studies demonstrate that down-regulation of HSP47 through RNA interference (RNAi) resulted in decrease in collagen deposition, amelioration of fibrosis and restoration of organ function in different disease models, such as liver fibrosis [13], pulmonary fibrosis [14], skin fibrosis [15] and dry eye syndrome in chronic graft-versus-host disease (GVHD) [16].

Immunohistochemistry demonstrated the co-expression of HSP47 and procollagen (Type I) in the pneumocytes (Type II) and myofibroblasts in patient samples with usual interstitial pneumonia. Evidence has revealed the increased expression of HSP47 in fibrotic lesions of IPF and other pulmonary disorders with diffuse alveolar damage [17]. HSP47 was detected in the serum of patients with acutely exacerbated IPF [18]. Myofibroblasts, through the production of HSP47-associated regulation of type I procollagen, play an important role in the progression of pulmonary fibrosis [19].

However direct evidence supporting the involvement of HSP47 in the EMT process and its role in the development and progression of lung fibrosis is not available. The present study evaluates whether HSP47 regulates the EMT process during formation of fibrotic tissue and disease progression in rat lung fibrosis models.

ND-L02-s0201 is a lipid nanoparticle (LNP) formulation that incorporates 6 key lipid components, encapsulating a synthetic small interfering ribonucleic acid (siRNA) active ingredient, NDT-05-0038. The LNP includes a retinoid-conjugated targeting agent (di-retinamide-PEG-di-retinamide), which promotes uptake by target cells (hepatic stellate cells for liver fibrosis or lung myofibroblasts for IPF). The active pharmaceutical ingredient NDT-05-0038 is a nuclease resistant, synthetic, double-stranded siRNA designed to reversibly inhibit the expression of HSP47 by targeting the homologous sequence across human, rat and mouse. Multiple clinical trials have evaluated the safety, tolerability and pharmacokinetics of ND-L02-s0201 in healthy volunteers and in subjects with liver fibrosis. In general, ND-L02-s0201 was well tolerated in the five completed clinical studies (three in healthy subjects [20] [21] [22] and two in subjects with liver fibrosis [23] or pulmonary fibrosis [24]). Biological activities were observed with improvements in efficacy studies in progressive hepatic fibrosis (METAVIR F3-4) noted in METAVIR, Ishak, and Knodell fibrosis scores, as well as decreased stiffness by FibroScan® at Week 5 [23]. In 2018, JUNIPER: a phase II study to evaluate the safety, biological activity, and PK of ND-L02-s0201 in subjects with IPF was initiated due to the encouraging early signs of efficacy in advanced liver fibrosis, preclinical efficacy in IPF models and significant unmet medical need in IPF patients.

We describe here the preclinical efficacy of ND-L02-s0201 in lung fibrosis resolution in several animal models with demonstrated progressive fibrosis over a range of study durations. These studies evaluated the effect of knockdown of the target gene, HSP47, on lung fibrosis resolution through biochemical and histological examinations as well as functional recovery through treadmill assessments.

Materials and Methods

ND-L02-s0201

ND-L02-s0201 was manufactured containing six key lipids in the composition, including the cationic, helper, and targeting lipids besides siRNA (NDT-05-0038), the active pharmaceutical ingredient. Particles were prepared using an ethanol injection process by combining an ethanolic solution of the lipids with an aqueous solution of siRNA. The final buffer composition of ND-L02-s0201 consisted of NDT-05-0038/lipid nanoparticles in 20 mM HEPES with a 9% sucrose buffer. Lipid composition and their respective molar ratios, siRNA : lipid ratio were developed to optimize drug loading capacity, potency, and product safety. The effect of each process parameter on key drug product quality attributes such as particle size, stability, and nucleic acid encapsulation, as well as *in vitro* and *in vivo* efficacy was determined. All the dosing concentrations in the studies described for ND-L02-s0201 refers to the concentration of NDT-05-0038.

Animals

Sprague-Dawley rats (250-280 g) were purchased from Charles River Laboratories. The animals were housed in standard caging systems under an alternating 12-hour light/dark

cycle, temperature at 18 - 26 ℃ and humidity at 30 - 70%. Animals were provided certified standard fresh rodent chow and tap water *ad libitum*. All animal involving procedures were approved by the Institutional Animal Care and Use Committees (IACUC) at Explora Biolabs (San Diego, CA 92109).

Rat model of bleomycin (BLM)-induced lung fibrosis

The animal body weight was 300 - 350 g at the initial BLM treatment. BLM (APP Pharmaceuticals, LLC. Schaumberg, IL 60173) was diluted in 0.9% saline for oropharyngeal (OP) aspiration at a final concentration of 6 mg/mL or 2 mg/mL for 3 mg/kg or 1 mg/kg application respectively. BLM induction was initiated at 3 mg/kg on Day 0, followed by 1 mg/kg on Days 1 - 6 for the first week. Subsequent BLM boost was conducted at 3 mg/kg once on Day 14 for the five-week model or five times on Day 14, 28, 42, 56, and 70 for the ten-week model [25].

Rat model of silica-induced lung fibrosis

Min-U-Sil5 silica powder (a gift from US Silica Corporation, Frederick, MD 21701) was suspended in 0.9% saline for OP aspiration at the final concentration of 83.3 mg/mL. Silica was administrated at 25 mg/g lung [26] on Days 0, 1, 2, 14, 28, and 42. Silica induction was conducted using same procedure described above for BLM induction. Silica suspension was mixed thoroughly before each administration.

Collagen content

Quantification of lung collagen amount was conducted following the modified procedure [27]. A slice of lung tissue from right interior lobe (100 - 150 mg of wet

weight) were used in hydroxyproline (HP) assay. Briefly the lung slices were hydrolyzed in 6 N hydrochloride (HCl) at 110^{o}C overnight followed by incubation with 4-dimethylamino-benzaldehyde for 25 min at 65°C, and absorbance of oxidized HP was determined at 558 nm. The amount of collagen was calculated based on standard curve generated in parallel and expressed in micrograms per lung based on the total wet lung weight.

Primary cell isolation/enrichment and characterization

Isolation of subsets of different cell types was conducted following the procedure with certain modifications [28] [29]. Briefly, alveolar macrophages were collected by repeated intratracheal lavage with 5 mM EDTA in D-PBS following cardiac perfusion. Isolation/enrichment of subpopulations of endothelial, epithelial or myofibroblast were achieved through gradient centrifugation following enzymatic digestion. Characterization of each cell populations was conducted through Q-PCR with gene-specific probes, EPCAM (Rn01473202_m1) for epithelial, ICAM2 (Rn01461346_m1) for endothelial, ACTA2 (Rn01759928_g1) for myofibroblast and PTPRC (CD45) (Rn00709901_m1) for macrophage (Thermo-Fisher).

Subset of animals from each group (six from Sham, five from BLM and six from BLM + ND-L02-s0201) were applied for correlation identification between fibrotic severity and enrichment of different cell populations. Left lungs were collected for histopathology evaluation and right lungs for cell fractionation.

Real-time PCR

Quantification of HSP-47 through real-time PCR was conducted following the

instruction provided by the manufacturer. Total RNA was extracted from a section of right caudal lobe of lung tissue or from isolated cell fractions described above using RNeasy columns (Qiagen, 74106) and adjusted to 10 ng/μL. Real-time PCR was performed on the ViiA7 system in triplicate using the TaqMan Gene Expression Master Mix (Applied Biosystems, 4369510). The relative gene expression was presented as fold-change of each gene of interest (GOI) compared to the Sham Group (designated as 1) for the following GOIs: ACTA2 (Rn01759928_g1), EPCAM (Rn01473202_m1), ICAM2 (Rn01461346_m1), and PTPRC (CD45) (Rn00709901_m1), Serpinh1 (HSP47, Rn0567777_m1), MRPL19 (Rn01425270_m1).

Rat fibrosis RT^2 profiler PCR array

Satellite animals from each group were used for characterization of the gene expression which were reported involving in lung fibrosis initiation and development. Six rats were selected from Group BLM-treated alone (fibrotic score 3-4, trichrome staining) and six rats from Group BLM + ND-L02-s0201 (fibrotic score 1), four rats from Sham Group were applied as control. A panel of 84 key fibrosis related genes were assessed with rat Fibrosis RT^2 Profiler PCR Arrays Kit (Qiagen, 330231). Briefly the first strand cDNA was synthesized with 100 ng total RNA in a 20 μL reaction volume with RT^2 First Strand Kit (Qiagen, 330404) and followed by amplification with RT^2 SYBR Green Q-PCR Master Mix (Qiagen, 330521) in a 384-well plate format. Raw data was exported and analyzed using the integrated web-based automated software for RT^2 profiler PCR Array data analysis which was available through Qiagen at http://www.qiagen.com/us/shop/genes-and-pathways/data-analysis-center-overview-page.

Histopathology

Left lung tissues were fixed with PBS neutralized 10% paraformaldehyde and sectioned (4 - 6 microns) and processed with H&E or Masson's trichrome stain for histopathology assessment at Wax-it Histology Services, Inc. (Vancouver, Canada). The slides were evaluated by a US Board certified pathologist at Nova Pathology (Vancouver, Canada) in a semi-quantitative manner, including key parameters of atelectasis, bronchiectasis, alveolar/interstitial edema, alveolar emphysema, pulmonary fibrosis, alveolar hemorrhage, hyperplasia of Type II alveolar epithelial cells, epithelial hypertrophy/hyperplasia of distal airways, alveolar macrophage infiltration and interstitial/airway inflammation, with severity score based on the following system: minimal = 1, mild = 2, moderate = 3 and marked = 4.

Epithelial-mesenchymal transition study

Single cell suspensions from naïve Sprague-Dawley rat (100-200g) lung tissue were produced through enzymatic digestion and gradient centrifugation following the procedure with certain modifications [28] [29]. The resulting cell pellets were panning on rat IgG pre-coated petri dish at 37℃ for thirty minutes. Unattached cells were collected and rinsed and seeded on collagen pre-coated 10 cm dishes in the medium of DMEM containing 10% FBS, at $1x10^6$/mL. Following initial forty-eight hours, cells were fractionated into 75 mm^2 flasks at $2x10^6$/flask. BLM induction was conducted four-hour following seeding on Day 0 at 2 mg/mL. After twenty-four hours the cell cultures were switched to freshly prepared medium supplemented with 50 nM ND-L02-s0201 and continuing culture for another two hours. Afterwards the cell cultures were switched back to the fresh medium containing 0.2 mg/mL BLM for

additional designated period. Characterization of cell population following the treatments was conducted on Days 0, 3, 4, 5 and 7 through FACS (BD Accuri™ C6) using immunostaining with anti α-SMA-FITC (Abcam, ab8211) and anti E-cadherin-Alexa 647 (BD, 560062).

Treadmill training and testing

Treadmill training and test were conducted on the treadmill device (Panlab, LE8710RTS). Animal qualification for the treadmill test was the completion of running distance > 20 meters for the last minute at the belt speed at 60 cm/sec during a seven-minute training session. A total of 30 rats selected from training session were randomized into three groups, ten rats were assigned to the Sham group, and the other 20 rats were assigned for BLM induction. More than 80% pre-trained Sham group animals were able to complete the total seven-minute running duration at 60 cm/sec with no signs of exhaustion. SEDACOM software (Panlab/Harvard Apparatus) was used to visualize and data exportation of running capacity endurance for further analysis.

Data Analysis

Statistical analysis was performed for assays which contained three or more groups ($n \geq 3$), using one-way ANOVA followed by Dunn's multiple comparisons *post hoc* test to determine if there were statistically significant differences observed between the mean or median values between groups. Unless otherwise specified, multigroup analysis evaluated treatment groups as compared to vehicle groups. For assays in which two groups were compared, non-paired *t* test was used for statistical analysis. For all

analyses, P values less than 0.05 were considered statistically significant (* $P < 0.05$, ** $P < 0.01$, *** $P < 0.001$ and **** $P < 0.0001$).

Results

ND-L02-s0201 treatment resulted in resolution of lung fibrosis in optimized BLM model in rats

The aim of this study was to evaluate the therapeutic effects of ND-L02-s0201 in an optimized BLM-induced rat model. BLM induction followed the protocol of Egger [30] with certain modifications to avoid significant spontaneous recovery and to ensure the persistence of formation of fibrotic tissue throughout the study. Validation of the BLM model was conducted through assessments of relative lung weight, whole HP content, and histopathological analysis (Supplement Fig.1). In the BLM model shown in Supplement Fig. 1A, compared to Sham Group (open bar), repeated OP aspiration of BLM in the Vehicle Group resulted in severe lung damage reflected by increased relative lung weight (Supplement Fig. 1B), elevated collagen (HP content) deposition in lung tissue (Supplement Fig. 1C), and substantial increase in histopathological scores (Supplement Fig. 1D). Excessive collagen deposition was further confirmed through trichrome staining (Supplement Fig. 1E) at the end of the study (Day 49), five weeks following the final dose of BLM on Day 14.

BLM-treated animals received ND-L02-s0201 treatment intravenously (IV) at an initial dose of 2 mg/kg on Day 18 and followed by subsequent weekly (QW) doses at 2, 1.5, 1 or 0.5 mg/kg. ND-L02-s0201 treatment resulted in statistically significant fibrosis resolution in a dose-dependent manner, including restoration of relative lung weight,

reduction of HP content and histological and trichrome scores (Fig 1B-E). Single initial dose of 2 mg/kg followed by 1.5 mg/kg, QW x four weeks led to statistically significant lung fibrosis resolution.

Gene array analysis demonstrated an up-regulation of a set of genes involved in collagen synthesis/deposition and fibrosis formation following BLM induction. ND-L02-s0201, at an initial dose of 2 mg/kg followed by 1.5 mg/kg, QW x four weeks, led to the reversal of the increase in the expression of these genes in addition to the siRNA target gene HSP47 (Fig 1G-H). Q-PCR results for the comparison of the full panel of 84 genes in the array are shown in Supplement Tab 1.

Cellular update of ND-L02-s0201

Characterization of cellular update was conducted with fluorescent labeled ND-L02-s0201 in BLM rat model. Colocalization assessment demonstrates that formulation promotes the uptake into myofibroblasts as well as additional cell types like alveolar type-2 cells which can transform into myofibroblasts (Supplement Fig. 2).

Down-regulation of α-SMA expression through inhibition of HSP47 in BLM treatment rat lung tissue

To evaluate the effect of HSP47 downregulation on α-SMA, image quantification analyses of the anti-HSP47 or α-SMA IHC staining from the sequential sections of lung tissue from the study presented in Fig. 1 was conducted. As shown in Supplement Fig. 8, BLM induction in Vehicle Group caused substantial elevation in both HSP47 and α-SMA expression and ND-L02-s0201 treatment led the reductions in both HSP47 and α-SMA (Supplement Fig. 8A, 8B). Representative images are presented in Supplement Fig. 8. Image alignment of anti HSP47 and α-SMA staining from the sequential sections

demonstrates clear co-localization between them. Furthermore, there was a good correlation between the two staining ($R^2 = 0.6162$, $P < 0.0001$) (Supplement Fig. 8C).

Reversal of BLM-induced accumulation of myofibroblasts and accelerated EMT through down-regulation of HSP47

Ex vivo evaluations were conducted to further understand the roles of different cell types during fibrotic formation and progression using primary cells from BLM treated rat lung tissue. Four different cell types (*i.e.*, myofibroblast, endothelial, epithelial, and macrophage) were enriched and characterized through specific gene marker analysis (Supplement Fig 3). Q-PCR data demonstrated myofibroblasts showed the highest level of HSP47 expression among the four cell types. BLM induction did not result in the elevation of HSP47 mRNA levels in any cell types (Fig. 2A). Instead increases in cell number were observed following BLM induction, more prominently in myofibroblasts (more than five folds) and less significantly among other cell types (Supplement Fig 4). Correlation analysis demonstrated a statistically significant relationship between myofibroblast cell numbers and lung weight with $R^2 = 0.556$ (Supplement Fig 6). ND-L02-s0201 treatment resulted in substantial reduction of myofibroblast counts towards the level of Sham Group (Fig. 2B). The myofibroblast cell counts also correlated to the tissue fibrosis scores through correlation statistical analysis ($R^2 = 0.688$, $n = 6$) (Fig. 2C). Dose-dependent down-regulation of HSP47 in the primary myofibroblasts was observed following ND-L02-s0201 treatment with estimated EC50 of 13 nM (Fig 2D).

Influence of HSP47 on EMT was further evaluated in primary epithelial cells from lung tissue. As shown in Fig 2E, epithelial cells displayed a natural course of EMT in culture

by Day 3-7 with reduced E-cad positive cells (solid line, filled circle) and increased α-SMA positive cells (dotted line, open circle). EMT process was accelerated following BLM induction evidenced by left shifting of both E-cad and α-SMA curves. This acceleration was reversed following 24 hours treatment with 50 nM ND-L02-s0201 (Fig 2F). Complete FACS analysis of all cell samples on Days 0, 3, 4, 5, 6, and 7 following BLM and ND-L02-s0201 treatment were shown in Supplement Fig 5.

ND-L02-s0201 treatment in chronic rodent models of IPF demonstrates statistically significant improvement in fibrosis

Therapeutic effects of ND-L02-s0201 in a clinically preferred biweekly (Q2W) dosing frequency were investigated in comparison with QW regimen in both chronic BLM model and the silica-induced fibrotic model.

In the chronic bleomycin model, additional four BLM inductions were conducted on Days 28, 42, 56, and 70. Anti-fibrotic effects of ND-L02-s0201were assessed in an extended duration of 12 weeks with the regimen either QW (ten total doses) or Q2W (five total doses) (Fig 3A). Compared to the Sham Group, the lung fibrotic changes in the Vehicle Group were maintained through the extended period (HP content and histopathology parameters). As presented in Fig 3B-D, a trend towards dose-dependent decrease in HP content and histopathology improvement were observed following ND-L02-s0201 treatment compared to the Vehicle Group. Similar therapeutic potency was achieved at Q2W regimen in comparison to QW when an approximate total drug was given (Fig 3E-G). There were no statistical differences in total HP content and trichrome scores between groups, Q2W, 3 mg/kg x five weeks compared to QW, 2 mg/kg x ten weeks or QW, 3 mg/kg x ten weeks ($P > 0.05$, *t*-test, two-tailed).

Silicosis, a common form of occupational lung disease, is caused by inhalation of crystalline silica dust and leads to inflammation, fibrosis, and nodular legions in the lung. As shown in Figure 4, a silica-induced lung fibrotic model was developed in rats with repeated OP aspiration of silica suspension of 25 mg/g lung. Following silica administration, animals in Vehicle Group showed progressively enlarged lungs in a time-course dependent manner from Day 21-101 as well as alterations in other relevant fibrotic parameters (Fig. 4 B-E).

Anti-fibrotic effects of ND-L02-s0201 in the silica model was evaluated at 2 mg/kg, QW with different treatment durations (Fig. 4F-I). Even though the numerical reduction of HP level did not reach statistical significance, all treatment groups showed remarkable decreases in histopathological and trichrome scores. Comparison between Q2W and QW demonstrated a similar anti-fibrotic potency at equivalent total dosage of 20 mg/kg over ten-week duration (4 mg/kg x five weeks or 2 mg/kg x ten weeks), reflected by reduction in HP level and improvement in histopathology and trichrome scores and the restoration of relative lung weight (Fig. 4 J-K).

ND-L02-s0201 treatment leads to the recovery of pulmonary function in BLM-treated rats

Impact of ND-L02-s0201 on pulmonary function in the BLM-induced rats was assessed by evaluating the running endurance on a treadmill. Animals were stratified into two groups, Sham and BLM, following the training phase targeting equivalent ability to consistently complete the treadmill testing at 60 cm/second with the final minute of running covering a distance exceeding 20 meters (Fig. 5A). BLM induction resulted in significant reduction in total running distance starting Day 16 compared to the Sham

Group, demonstrating an impact on lung function. BLM-treated rats were further stratified into two groups (Vehicle and ND-L02-s0201 treatment) based on Day 16 data (Fig. 5B). ND-L02-s0201 treatment was initiated on Day 18 at 2 mg/kg, QW for four weeks. As shown in Fig 5D, the Vehicle Group animals showed further decline in running capacity Days 18 – 23 and sustained poor running endurance throughout the study. Animals receiving ND-L02-s0201 showed improved performance on the treadmill for the remaining testing period. Day 49 the final test showed significant reduction in running capacity of animals in the Vehicle Group compared to the Sham Group ($P < 0.0001$, unpaired *t*-test), confirming the detrimental impact of BLM induction on the lung function. Animals following ND-L02-s0201 treatment demonstrated statistically significant improvement in running capacity compared to the Vehicle group ($P < 0.05$). No statistically significant difference between the ND-L02-s0201 treatment and Sham Groups ($P > 0.05$) (Fig. 5E).

Treadmill test has been implemented as key parameter for cardiopulmonary function assessment to evaluate the degree of impairment in heart, lung, or skeletal muscle system. In considering the local (OP) administration of BLM in this study and the lack of BLM-related cardiac or skeletal muscle dysfunction which were assessed by an independent board-certified pathologist, we believe the improvement in running endurance following the treatment of ND-L02-s0201 was mainly due to the resolution of pulmonary functions rather than improvement in other unlikely toxicities caused by BLM treatment. There was no substantial body weight loss among the groups towards to the end of course of treadmill tests (Supplement Fig. 7). These results provide strong evidence that ND-L02-s0201 treatment can benefit the pulmonary function recovery in the BLM induced lung fibrosis model.

Discussion

In view of the limited number of therapeutic options which slow disease progression and the progressive course of the illness, there exists a tremendous unmet medical need for highly effective and well-tolerated agents that halt, or ideally reverse, the fibrosis in IPF patients. Progress in the understanding of the pathophysiology has led to the development of novel experimental therapeutics. For example, inhibition of aberrant fibroblastic proliferation and accumulation of ECM proteins such as collagen have become the focus of current therapeutic studies for IPF [31]. HSP47 is a key molecular chaperone that facilitates collagen triple helix formation and is critical for collagen formation. Studies utilizing pulmonary fibrosis clinical samples evidenced with the increase in HSP47 expression in lung tissue and plasma [19] [17] [18] [32] as well as co-localization of HSP47 and type I procollagen in type II pneumocytes and myofibroblasts in usual interstitial pneumonia [19] led to great interest in developing novel therapeutics through inhibition of HSP47 as an approach to control aberrant production of collagen [33].

ND-L02-s0201 is a drug product designed to down-regulate HSP47 specifically and result in the reduction of collagen synthesis and deposition. In present study ND-L02-s0201 treatment led to substantial reduction of HSP47 associated with a decrease in HP content and improvement of histological parameters as well as restoration of relative organ weight in rat fibrotic models. Not surprisingly a series of pro-fibrotic genes were up-regulated following BLM induction, which are relevant to collagen synthesis/secretion and fibrosis development. Following ND-L02-s0201

treatment the increases of the gene expressions were reversed, which was considered through inhibition of HSP47 (named Serpinh1 in the array, Fig. 1H, Supplement Tab 1). Further investigations need to be conducted to address the mechanisms of the regulation of pro-fibrotic genes through HSP47 machinery.

Serving as a key source of excess production of collagenous ECM [34] myofibroblasts are fundamental drivers in the development and progression in IPF and therefore are of great interest in both research and development of novel therapeutics for IPF treatment. Multiple sources of myofibroblast recruitment and accumulation have been identified. Additionally, activated myofibroblasts demonstrate augmented proliferation and resistance to programmed cell death [35].

During EMT the epithelial cells express distinct mesenchymal markers and lose epithelial markers as well as apicobasal polarity and intercellular junctions. Alteration of cell polarity and adhesion results in the disruption of basement membrane and facilitates epithelial cell penetration of the ECM-rich compartment [36]. In the present study the increase in the myofibroblast population was more prominent compared to all other cell types. This increase was positively correlated to the relative lung weight gain as well as severity of the fibrotic score. *In vitro* assay with primary rat epithelial cells exposed to BLM showed facilitation of the transition from epithelial to myofibroblast phenotype. Further analysis demonstrated myofibroblasts had the highest HSP47 expression which was not increased further following BLM treatment. The elevated expression of HSP47 following BLM treatment was mainly attributed to the increase in myofibroblast numbers

instead of the expression level in the cells. Down-regulation of HSP47 through ND-L02-s0201 treatment successfully prevented the progression of EMT both *in vivo* and *in vitro*. To our knowledge this is the first study that provides direct evidence inhibition of HSP47 can prevent progression of lung fibrosis through EMT suppression. It has been reported by other laboratories that down-regulation of HSP47 resulted in endoplasmic reticulum (ER) stress-mediated apoptosis of fibroblasts in cell culture [37] [38], which could also be the mechanism of anti-fibrotic effects of ND-L02-s0201.

BLM induced pulmonary fibrosis models have been widely used in preclinical studies of potential therapies development for IPF. Unfortunately, the drug candidates through BLM model assessment were unsuccessful due to inappropriate study settings. From 1980 to 2006, the majority of the studies (211 out of 221) were conducted in a post-exposure preventive regimen, in which the test drugs were given less than seven days after the last BLM dose [39]. It was also reported that spontaneous resolution of fibrosis occurred following a single BLM treatment and infrequent BLM treatment [40] [39]. To support ND-L02-s0201 pharmacological evaluation we have developed a robust BLM model with optimized induction regime through full assessments of tissue collagen deposition and histopathological endpoints. Substantial and persistent changes of lung fibrosis were up to eight weeks through multiple rounds of BLM administration in the chronic BLM models, which provided a sustained evaluation window for reliable efficacy studies. Dose-dependent anti-fibrotic effects of ND-L02-s0201 in this model were observed with QW dosing, reflected by restoration of relative lung weight, reduction in collagen content and amelioration in histopathological scores. In addition to the restoration of the structural integrity of lung tissue, improvement of pulmonary function

was also observed following ND-L02-s0201 treatment in the running endurance capacity test.

Anti-fibrotic effects of ND-L02-s0201 were observed in a silica-induced lung fibrosis model in rats. Following silica OP induction, the increase in lung HP content and histopathological changes sustained over three months without significant recovery. Intervention with ND-L02-s0201 resulted in amelioration of histopathological alterations and stopped the worsening of the fibrosis. As in the BLM model, ND-L02-s0201 Q2W treatment resulted in similar anti-fibrotic potency as a QW regimen in silica models. Data from both models, either BLM or silica, provide strong evidence supporting Q2W dosing of ND-L02-s0201 in IPF patients.

In conclusion, the results from the current studies provide evidence that down-regulation of HSP47 expression, a key protein supporting synthesis and deposition of properly folded collagen during lung tissue remodeling following injury, can inhibit the development of fibrosis, stop progression of disease and help restore pulmonary function. In addition to the direct role on collagen processing, down-regulation of HSP47 results in inhibition of EMT which leads to a reduction in myofibroblasts. Anti-fibrotic effects of ND-L02-s0201 have been demonstrated in both BLM-induced and silica-treated rat models, evidenced by the recovery of structural integrity of lung tissue as well as the improvement of pulmonary functions. Given the significant unmet medical need and the preclinical studies here as well as previous clinical studies in healthy volunteers and subjects with hepatic fibrosis, ND-L02-s0201 is now under evaluation in a Phase II clinical study in patients with IPF [41]. Further investigation can be conducted on

ND-L02-s0201 as therapeutic option for pulmonary fibrosis arising from different causes including viral infection such as COVI-19 disease [42].

References

[1] G. Raghu, "An official ATS/ERS/JRS/ALAT statement: idiopathic pulmonary fibrosis: evidence-based guidelines for diagnosis and management.," *Am J Respir Crit Care Med.,* vol. 183, no. 6, pp. 788-824, 15 Mar 2011.

[2] B. Ley, H. Collard and T. J. King, "Clinical course and prediction of survival in idiopathic pulmonary fibrosis," *Am J Respir Crit Care Med,* vol. 183, no. 4, pp. 431-40, 15 Feb 2011.

[3] M. Selman, T. King and A. Pardo, "Idiopathic pulmonary fibrosis: prevailing and evolving hypotheses about its pathogenesis and implications for therapy," *Ann Intern Med.,* pp. 136-51, 2001.

[4] V. Thannickal, G. Toews, E. White, J. 3. Lynch and F. Martinez, "Mechanisms of pulmonary fibrosis," *Annu Rev Med.,* pp. 395-417, 2004.

[5] F. Klingberg, B. Hinz and E. White, "The myofibroblast matrix: implications for tissue repair and fibrosis," *J Pathol.,* pp. 298-309, 2013.

[6] B. Willis, J. Liebler, K. Luby-Phelps, A. Nicholson, E. Crandall, R. du Bois and Z. Borok, "Induction of epithelial-mesenchymal transition in alveolar epithelial cells by transforming growth factor-beta1: potential role in idiopathic pulmonary fibrosis," *Am J Pathol.,* pp. 1321-32, 2005.

[7] B. Willis, R. duBois and B. Z. , "Epithelial origin of myofibroblasts during fibrosis in the lung," *Proc Am Thorac Soc.,* pp. 377-82, 2006.

[8] R. Reilkoff, R. Bucala and E. Herzog, "Fibrocytes: emerging effector cells in chronic inflammation," *Nat Rev Immunol.,* pp. 427-35, 2011.

[9] N. Hashimoto, S. Phan, K. Imaizumi, M. Matsuo, H. Nakashima, T. Kawabe, K. Shimokata and Y. Hasegawa, "Endothelial-mesenchymal transition in bleomycin-induced pulmonary fibrosis," *Am J Respir Cell Mol Biol.,* pp. 161-72, 2010.

[10] H. Masuda, M. Fukumoto, K. Hirayoshi and K. Nagata, "Coexpression of the collagen-binding stress protein HSP47 gene and the alpha 1(I) and alpha 1(III) collagen genes in carbon tetrachloride-induced rat liver fibrosis," *J Clin Invest.,* pp. 2481-8, 1994.

[11] T. T. Razzaque MS, "Collagen-binding heat shock protein (HSP) 47 expression in

anti-thymocyte serum (ATS)-induced glomerulonephritis," *J Pathol. ,* pp. 24-9, 1997.

[12] Y. Honzawa, H. Nakase, M. Shiokawa, T. Yoshino, H. Imaeda, M. Matsuura, Y. Kodama, H. Ikeuchi, A. Andoh, Y. Sakai, K. Nagata and T. Chiba, "Involvement of interleukin-17A-induced expression of heat shock protein 47 in intestinal fibrosis in Crohn's disease," *Gut,* pp. 1902-12, 2014.

[13] Y. Sato, K. Murase, J. Kato, K. T. Sato, Y. Kawano, R. T. Takimoto, K. Miyanishi, T. Matsunaga, T. Takayama and Y. Niitsu, "Resolution of liver cirrhosis using vitamin A-coupled liposomes to deliver siRNA against a collagen-specific chaperone," *Nat Biotechnol.,* pp. 431-42, 2008.

[14] M. Otsuka, M. Shiratori, H. Chiba, K. Kuronuma, Y. Sato, Y. Niitsu and H. Takahashi, "Treatment of pulmonary fibrosis with siRNA against a collagen-specific chaperone HSP47 in vitamin A-coupled liposomes," *Exp Lung Res.,* pp. 271-282, 2017.

[15] T. Yamakawa, H. Ohigashi, D. Hashimoto, E. Hayase, S. Takahashi, M. Miyazaki, K. Minomi, M. Onozawa, Y. Niitsu and T. Teshima, "Vitamin A-coupled liposomes containing siRNA against HSP47 ameliorate skin fibrosis in chronic graft-versus-host disease," *Blood,* pp. 1476-1485, 2018.

[16] H. Ohigashi, D. Hashimoto, E. Hayase, S. Takahashi, T. Ara, T. Yamakawa, J. Sugita, M. Onozawa, M. Nakagawa and T. Teshima, "Ocular instillation of vitamin A-coupled liposomes containing HSP47 siRNA ameliorates dry eye syndrome in chronic GVHD," *Blood Adv.,* pp. 1003-1010, 2019.

[17] T. Kakugawa, H. Mukae, T. Hayashi, H. Ishii, S. Nakayama, N. Sakamoto, S. Yoshioka, K. Sugiyama, M. Mine, Y. Mizuta and S. kohno, "Expression of HSP47 in Usual Interstitial Pneumonia and Nonspecific Interstitial Pneumonia," *Respir Res.,* vol. 6, no. 1, pp. 57-66, Jun 2005.

[18] T. Kakugawa, S. Yokota, Y. Ishimatsu , T. Hayashi, S. Nakashima , S. Hara, N. Sakamoto, Y. Matsuoka, H. Kubota , M. Mine , h. Mukae, K. Nagata and S. Kohno, "Serum heat shock protein 47 levels in patients with drug-induced lung disease.," *Respir Res.,* vol. 14, no. 1, pp. 133-143, 20 Nov 2013.

[19] T. Iwashita, J. Kadota, S. Naito, H. Kaida, Y. Ishimatsu, M. Miyazaki, Y. Ozono and S. Kohno, "Involvement of collagen-binding heat shock protein 47 and procollagen type I synthesis in idiopathic pulmonary fibrosis: contribution of type II pneumocytes to fibrosis.," *Hum Pathol.,* vol. 31, no. 12, pp. 1498-1505, Dec 2000.

[20] "https://clinicaltrials.gov/ct2/show/NCT01858935," [Online].

[21] "https://clinicaltrials.gov/ct2/show/NCT03241264," [Online].

[22] "https://www.clinicaltrials.gov/ct2/show/NCT01858935?term=BMS-986263&draw=2&rank=6," [Online].

[23] "https://clinicaltrials.gov/ct2/show/NCT02227459," [Online].

[24] "https://www.clinicaltrials.jp/cti-user/common/Top.jsp," [Online].

[25] A. Degryse, H. Tanjore, X. Xu, V. Polosukhin, B. Jones, F. McMahon and L. Gleaves, "Repetitive intratracheal bleomycin models several features of idiopathic pulmonary fibrosis.," *Am J Physiol Lung Cell Mol Physiol.,* vol. 299, no. 4, pp. 442-452, Oct 2010.

[26] V. Barbarin, A. Nihoul, P. Misson, M. Arras, M. Delos, I. Leclercq, D. Lison and F. Huaux, "The role of pro- and anti-inflammatory responses in silica-induced lung fibrosis.," *Respir Res.,* vol. 6, pp. 112-125, 7 Oct 2005.

[27] T. Hewitson and G. Becker, Kidney Research-experimental protocols, vol. 466, T. Hewitson and G. Becker, Eds., Springer, 2009, pp. 223-235.

[28] A. Bantikassegn, X. Song and K. Politi, "Isolation of epithelial, endothelial, and immune cells from lungs of transgenic mice with oncogene-induced lung adenocarcinomas," *Am J Respir Cell Mol Biol.,* vol. 52, no. 4, pp. 409-417, Apr 2015.

[29] R. Gonzalez and L. Dobbs, "Isolation and culture of alveolar epithelial Type I and Type II cells from rat lungs," *Methods Mol Biol.,* vol. 945, pp. 145-159, 2013.

[30] C. Egger , C. Cannet , C. Gérard, E. Jarman, G. Jarai, A. Feige, T. Suply, A. Micard, B. Tigani and N. Beckman, "Administration of bleomycin via the oropharyngeal aspiration route leads to sustained lung fibrosis in mice and rats as quantified by UTE-MRI and histology," *PLoS One.,* vol. 8, no. 5, p. e63432, 7 May 2013.

[31] T. J. King, A. Pardo and M. Selman, "Idiopathic pulmonary fibrosis," *Lancet.,* vol. 378, no. 9807, pp. 1949-1961, 3 Dec 2011.

[32] M. Amenomori, H. Mukae, N. Sakamoto, T. Kakugawa, T. Hayashi, A. Hara, S. Hara, H. Fujita, H. Ishimoto, Y. Ishimatsu, T. Nagayasu and S. Kohno, "HSP47 in lung fibroblasts is a predictor of survival in fibrotic nonspecific interstitial pneumonia," *Respir Med.,* vol. 104, no. 6, pp. 895-901, Jun 2010.

[33] T. Taguchi and M. Razzaque, "The collagen-specific molecular chaperone HSP47: is there a role in fibrosis?," *Trends Mol Med.,* vol. 13, no. 2, pp. 45-53, Feb 2007.

[34] B. Hinz, S. Phan, V. Thannickal, A. Galli, M. Bochaton-Piallat and G. Gabbiani, "The myofibroblast: one function, multiple origins," *Am J Pathol.,* pp. 1807-16, 2007.

[35] K. Kis, X. Liu and J. Hagood, "Myofibroblast differentiation and survial in fibrotic disease," *Expert Rev Mol Med,* vol. 13, p. e27, 2011.

[36] J. Lim and J. Thiery, "Epithelial-mesenchymal transitions: insights from development,"

Development., vol. 139, no. 19, pp. 3471-3486, Oct 2012.

[37] T. Miyamura, N. Sakamoto, T. Kakugawa, H. Taniguchi, Y. Akiyama, D. Okuno, S. Moriyama, A. Hara, T. I. Kido, H. Yamaguchi, T. Miyazaki, Y. Obase and Y. Ishima, "Small molecule inhibitor of HSP47 prevents pro-fibrotic mechanisms of fibroblasts in vitro," *Biochem Biophys Res Commun,* vol. 530, no. 3, pp. 561-565, 2020.

[38] K. Kawasaki, R. Ushioda, S. Ito, K. Ikeda, Y. Masago and K. Nagata, "Deletion of the collagen-specific molecular chaperone Hsp47 causes endoplasmic reticulum stress-mediated apoptosis of hepatic stellate cells," *J Biol Chem,* vol. 290, no. 6, pp. 3639-46, 2015.

[39] A. Moeller, K. Ask, D. Warburton, J. Gauldie and M. Kolb, "The bleomycin animal model: a useful tool to investigate treatment options for idiopathic pulmonary fibrosis?," *Int J Biochem Cell Biol.,* vol. 40, no. 3, pp. 362-282, 2008.

[40] M. Mouratis and V. Aidinis, "Modeling pulmonary fibrosis with bleomycin.," *Curr Opin in Pulm Med,* vol. 17, pp. 355-361, Sep 2011.

[41] clinicaltrials.gov, "JUNIPER: A Phase 2 Study to Evaluate the Safety, Biological Activity, and PK of ND-L02-s0201 in Subjects With IPF," 28 May 2018. [Online]. Available: https://clinicaltrials.gov/ct2/show/NCT03538301.

[42] A. S. Ojo, S. A. Balogun, O. T. Williams and O. S. and Ojo, "Pulmonary Fibrosis in COVID-19 Survivors: Predictive Factors and Risk Reduction Strategies," *Pulmonary Medicine,* pp. 1-10, 2020.

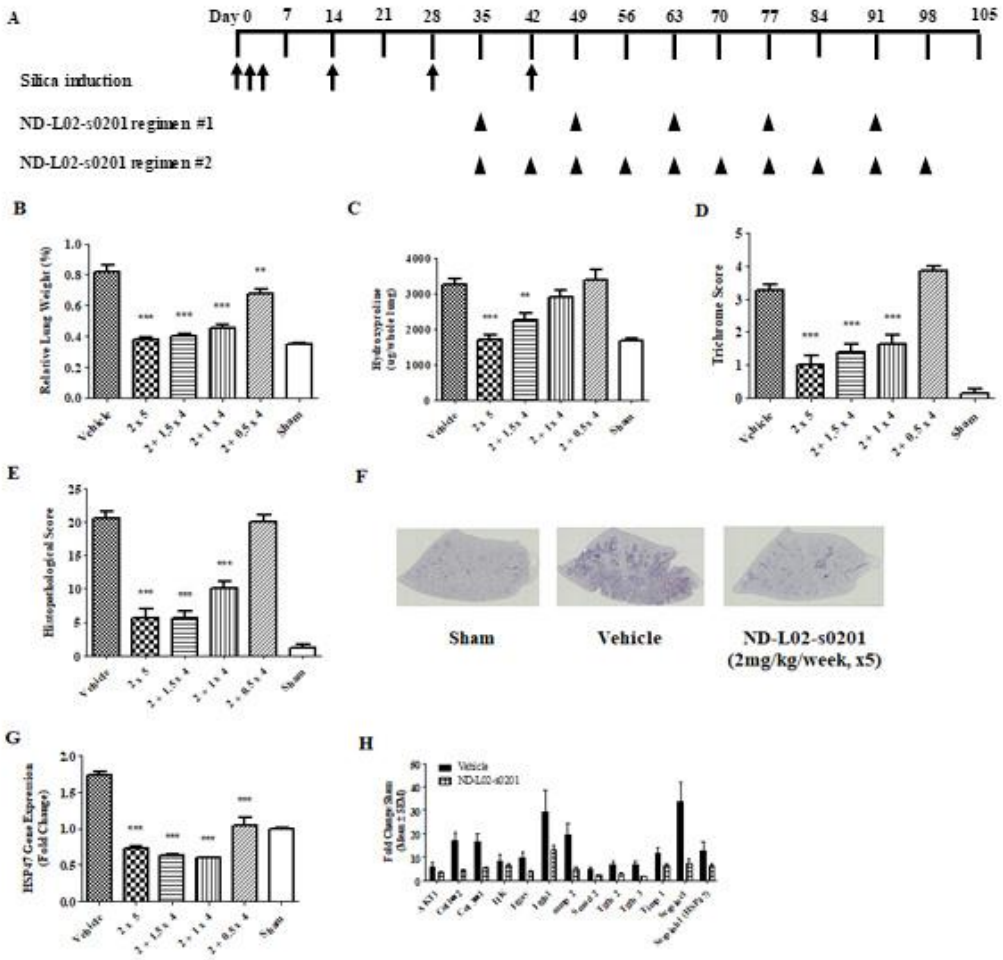
A
Day 0
7
14
21
28
35
42
49
56
63
70
77
84
91
98
105
Silica induction
ND-L02-s0201 regimen #1
ND-L02-s0201 regimen #2
B
Relative Lung Weight (%)
C
Hydroxyproline (ug/whole lung)
D
Trichrome Score
E
Histopathological Score
F
Sham
Vehicle
ND-L02-s0201
(2mg/kg/week, x5)
G
HSP-47 Gene Expression (Fold Change)
H
Vehicle
ND-L02-s0201
Fold Change Sham (Mean ± SEM)

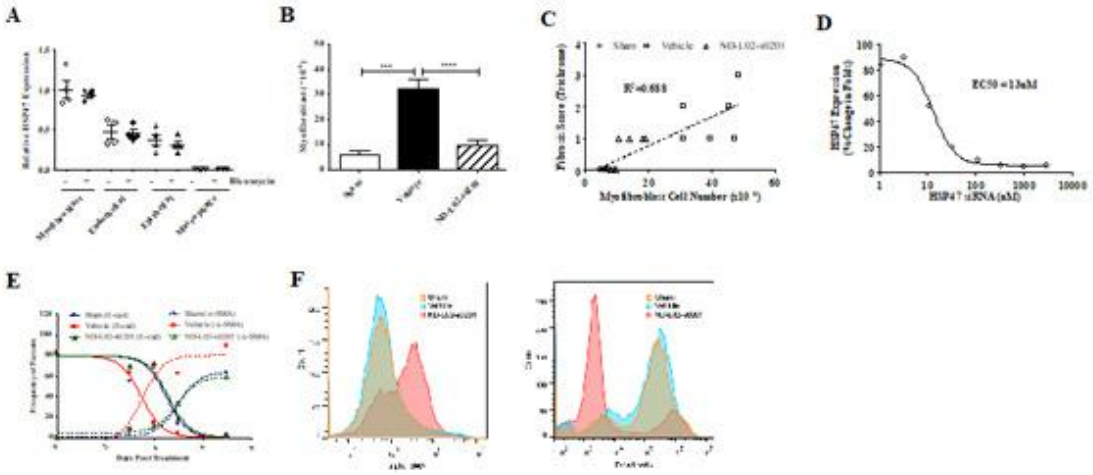
A
B
C
D
E
F
EC50 = 13nM
R² = 0.651

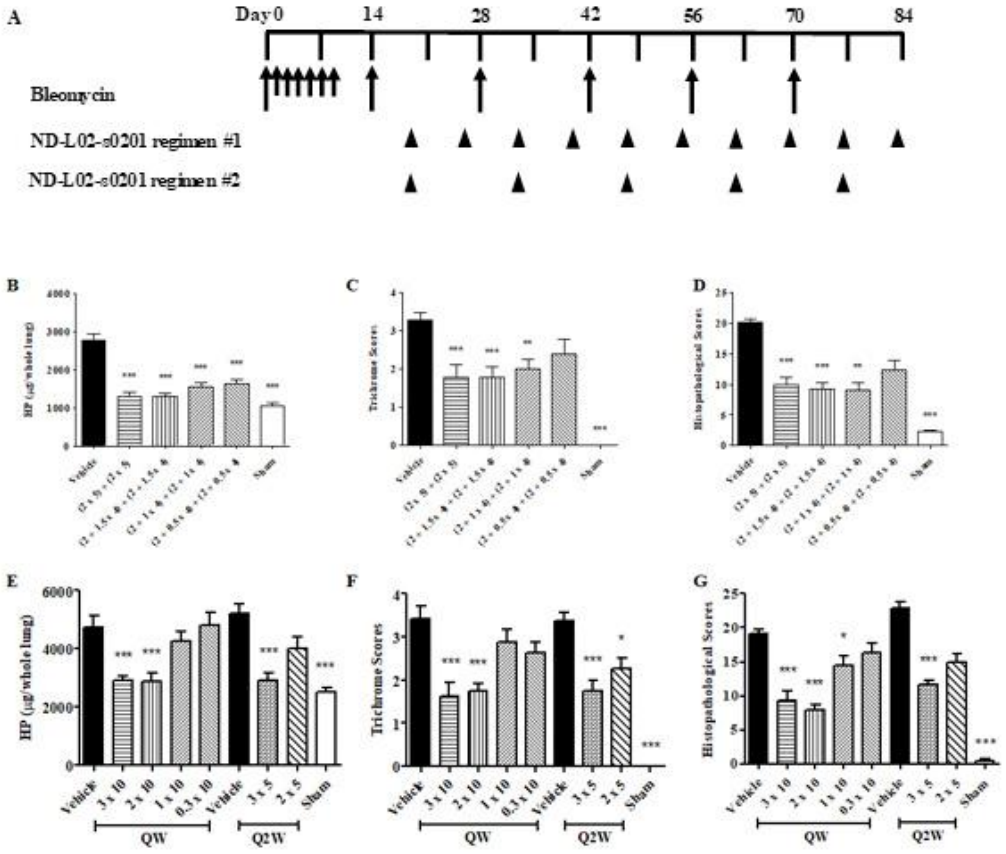
A
Day 0
14
28
42
56
70
84
Bleomycin
ND-L02-s0201 regimen #1
ND-L02-s0201 regimen #2
B
C
D
E
F
G
HP (μg/whole lung)
Trichrome Scores
Histopathological Scores
Vehicle
3 x 10
2 x 10
1 x 10
0.3 x 10
Vehicle
3 x 5
2 x 5
Sham
QW
Q2W

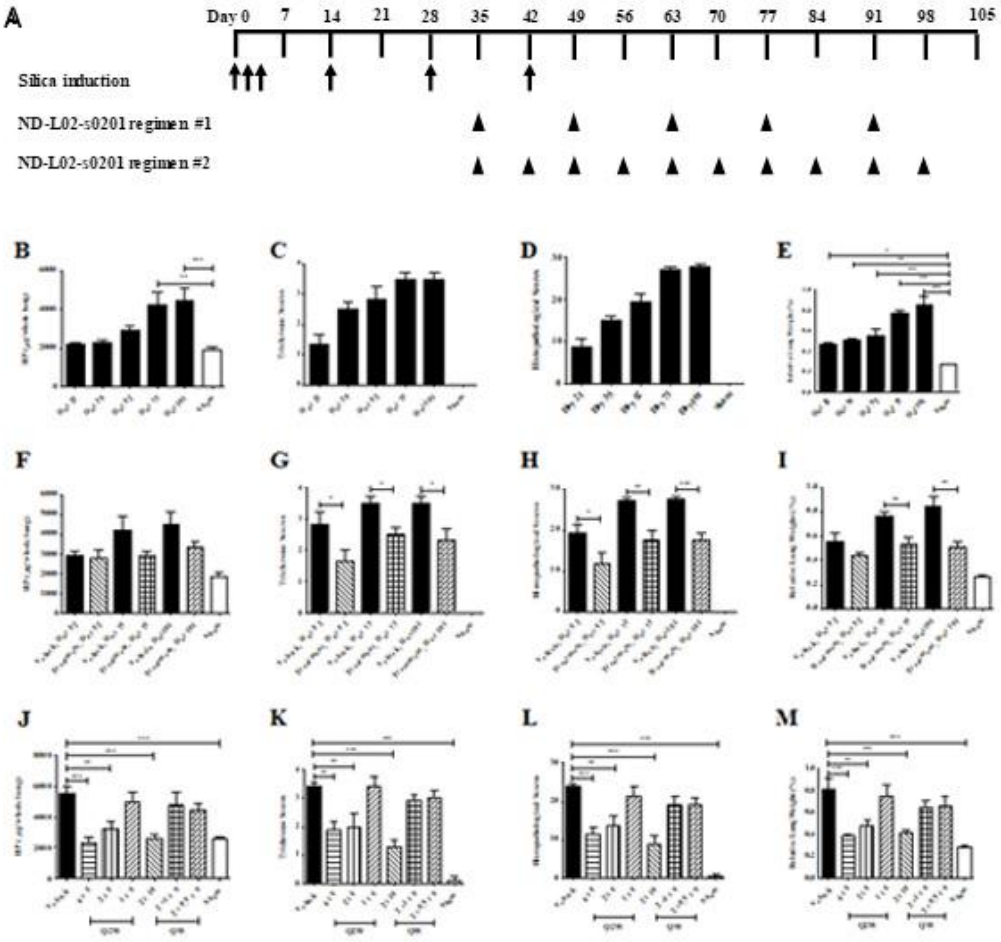
A
Day 0
7
14
21
28
35
42
49
56
63
70
77
84
91
98
105
Silica induction
ND-L02-s0201 regimen #1
ND-L02-s0201 regimen #2
B
C
D
E
F
G
H
I
J
K
L
M

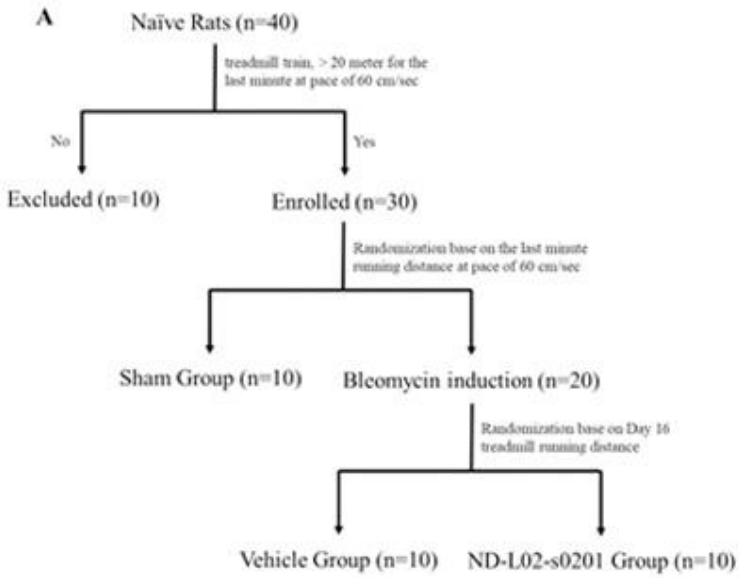
A
Naïve Rats (n=40)
treadmill train, > 20 meter for the last minute at pace of 60 cm/sec
No
Yes
Excluded (n=10)
Enrolled (n=30)
Randomization base on the last minute running distance at pace of 60 cm/sec
Sham Group (n=10)
Bleomycin induction (n=20)
Randomization base on Day 16 treadmill running distance
Vehicle Group (n=10)
ND-L02-s0201 Group (n=10)

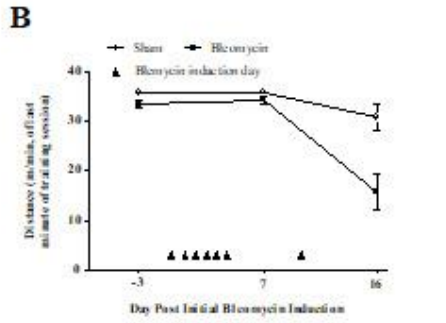
B
Sham
Bleomycin
Bleomycin induction day
Day Post Initial Bleomycin Induction

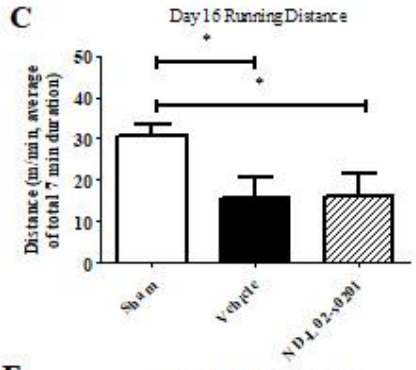
C
Day 16 Running Distance
Distance (m/min, average of total 7 min duration)
Sham
Vehicle
ND-L02-s0201

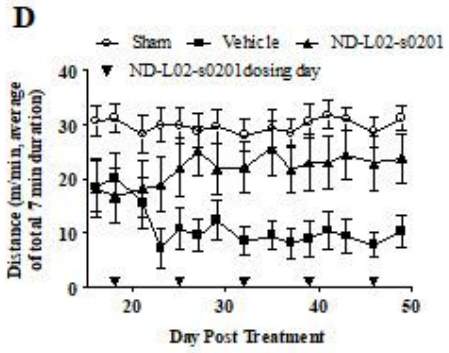
D
Sham
Vehicle
ND-L02-s0201
ND-L02-s0201dosing day
Distance (m/min, average of total 7 min duration)
Day Post Treatment

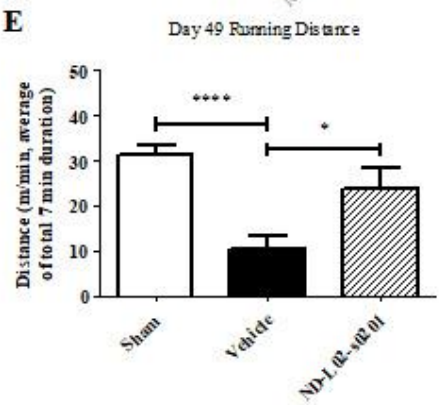
E
Day 49 Running Distance
Distance (m/min, average of total 7 min duration)
Sham
Vehicle
ND-L02-s0201

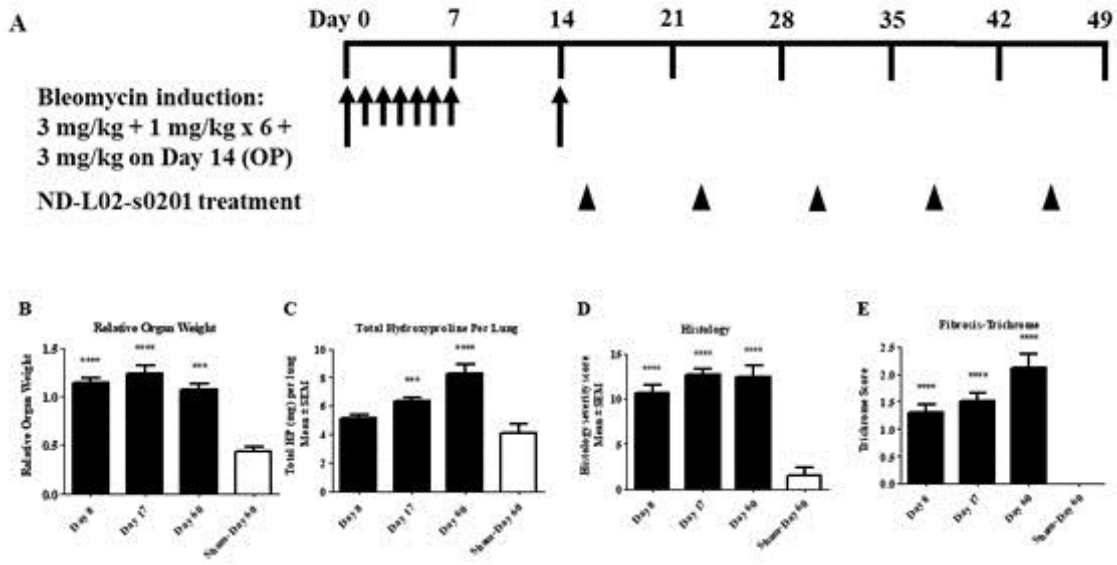

Supplement Fig. 1. BLM rat lung fibrosis model development and validation. (A) Male Sprague-Dawley rats were treated with BLM at 3 mg/kg (Day 0) followed by 1 mg/kg (Day 1 to 6) (0.5 mL/kg, OP) and boosted on Day 14 at 3 mg/kg. Subsets of animals were terminated on Day 6, 17 and 60 following BLM inductions respectively. Lung tissue collected from each animal were assessed on relative lung weight, collagen content, and fibrotic severity through histopathology evaluation. (B) Significantly increased relative lung weight was observed starting from Day 6 and throughout to Day 17 and 60. (C) Lung collagen deposition increased from Day 6 to 17 and 60, indicating the disease progression continued after the final doses of BLM on day 14. (D, E) Histopathology and Trichrome staining-based fibrosis evaluation confirmed this conclusion.

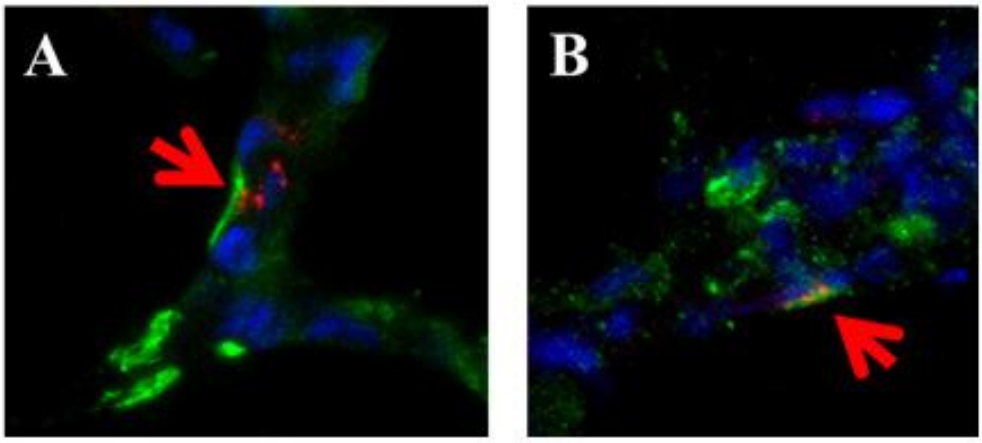

Supplement Fig. 2. Cellular uptake of ND-L02-s0201 in BLM treatment rat lung tissue. Male Sprague-Dawley rats were treated with BLM at 3 mg/kg (Day 0) followed by 1 mg/kg (Day 1 to 6) (0.5 mL/kg, OP) and boosted on Day 14 at 3 mg/kg. Animals received ND-L02-s0201 treatment once at 2 mg/kg and the tissue samples were collected four hours after injection for image process. Colocalization assessment demonstrates that formulation promoted the uptake into myofibroblasts as well as additional cell types like alveolar type-2 cells which can transform into myofibroblasts through EMT processing following BLM treatment. (A) ND-L02-s0201 with labeled siRNA (in red), fibroblasts visualized with anti α-SMA stain (in green), cell nuclei stained with DAPI (in blue). (B) ND-L02-s0201 with labeled siRNA (in red), alveolar type-2 visualized with anti proSP-C stain (in green), cell nuclei stained with DAPI (in blue).

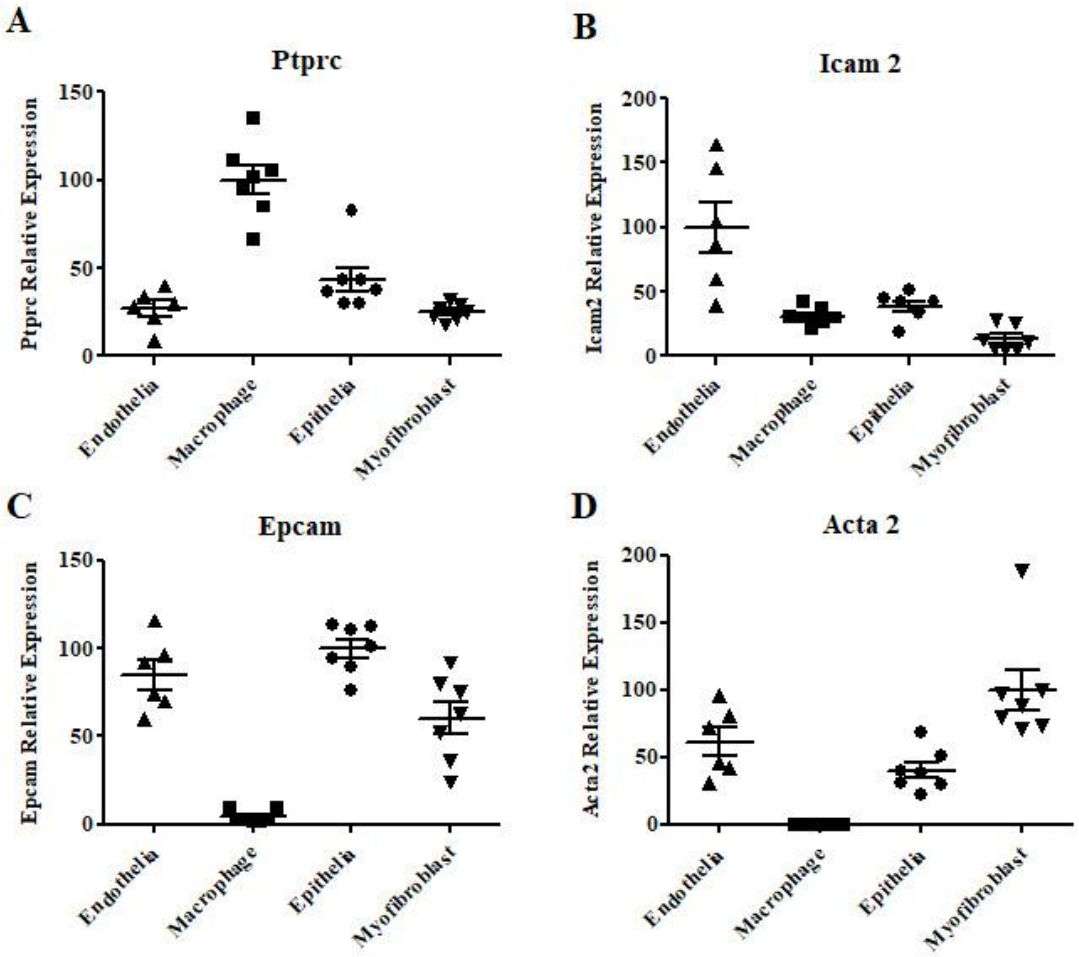

Supplement Fig. 3. Enrichment of cell subpopulation from lung tissue. For the four cell subpopulations isolated from naïve animals, Q-PCR analysis for four cell marker genes, (A) PTPRC (CD45) (Rn00709901_m1), (B) ICAM2 (Rn01461346_m1), (C) EPCAM (Rn01473202_m1), and (D) ACTA2 (Rn01759928_g1), were completed using housekeeping gene MRPL19 (Rn01425270_m1) as reference gene. As shown below, the relative expression levels for the respective gene marker were the highest among the four isolated cell populations, confirming the relative enrichment of the specific cell type following the cell isolation procedures.

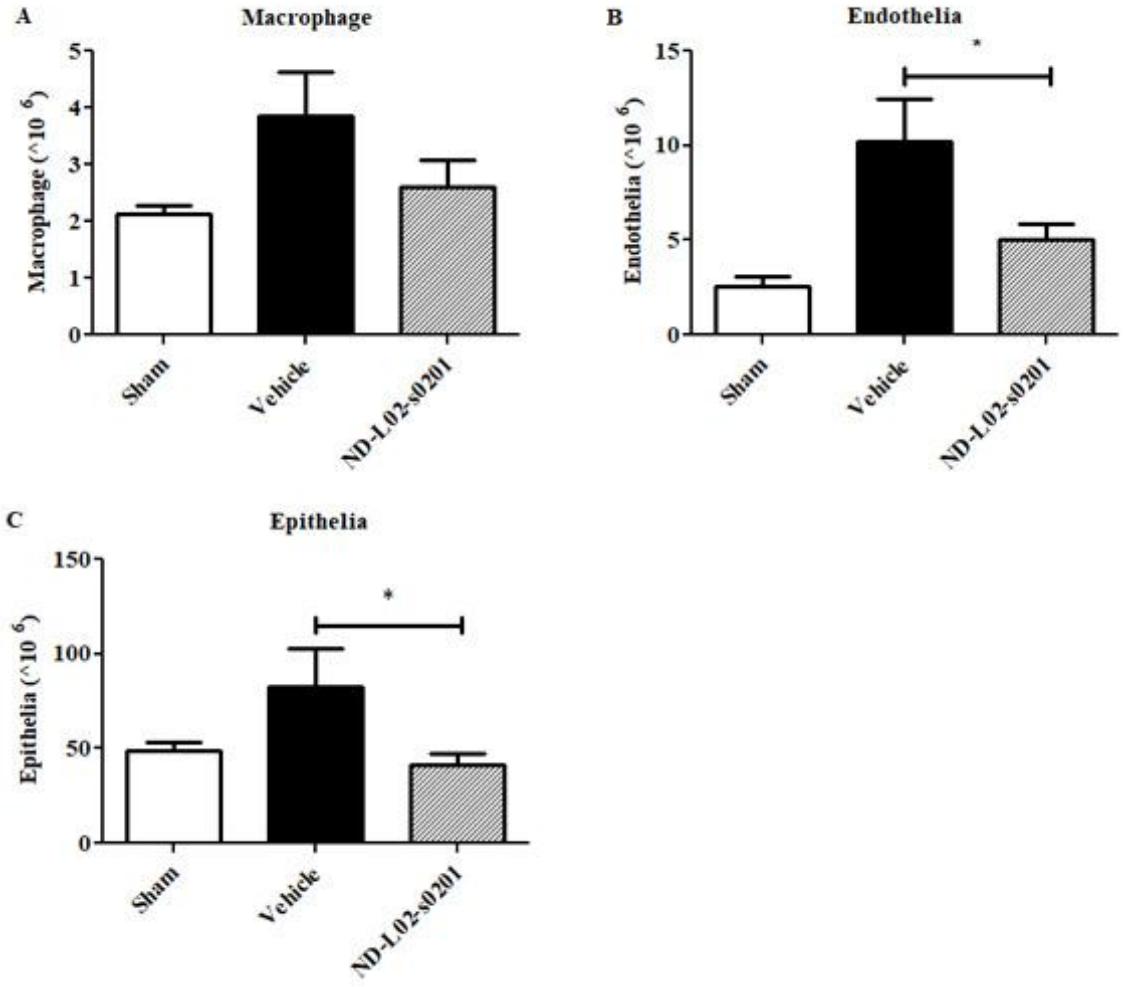

Supplement Fig. 4. Increase in cell populations following BLM induction. The increase in myofibroblasts was more prominent following BLM induction, approximate 5.2 folds related to the Sham Group (Fig. 2B). Comparatively the changes in other cell populations macrophage (A), endothelia (B) and epithelia (C) were less significant, 1.8, 3.9 or 1.7 folds related to the Sham Group respectively. ND-L02-s0201 treatment (2 mg/kg/week, four weeks) resulted in the reduction of myofibroblast counts by 60% related to the Vehicle Group, towards the level of the Sham Group (Fig. 2B).

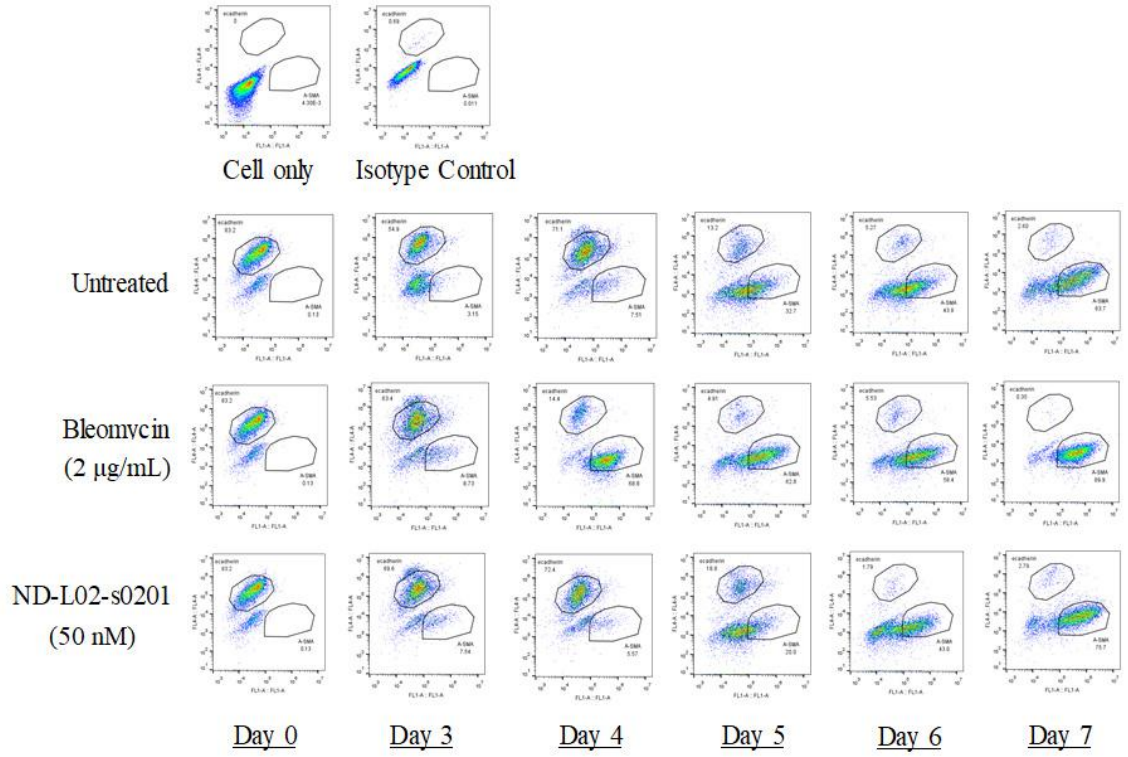

Supplement Fig. 5. EMT assay with primary rat epithelial cells. Culture of primary lung cells were treated with BLM and ND-L02-s0201 as described in Materials and Method. Anti α-SMA-FITC (Abcam, ab8211) and anti E-Cadherin-Alexa 647 (BD, 560062) double staining FACS (BD Accuri™ C6) were performed for cells collected from Day 0 and Days 3-7. Dot plot presented below showed distribution of E-cadherin positive (Y axis) and α-SMA positive (X axis) cells.

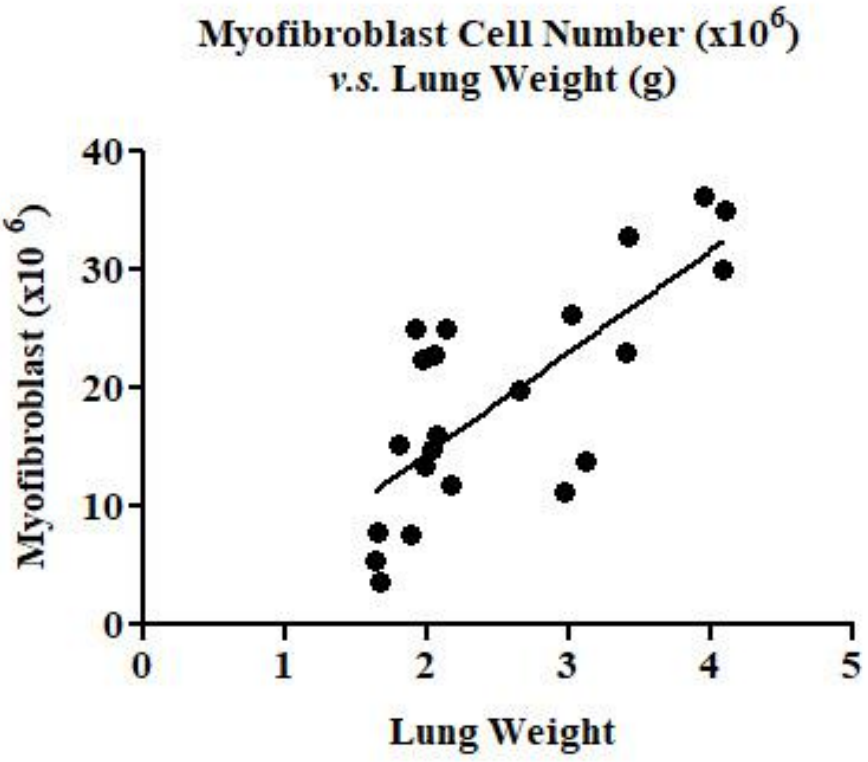

Number of XY Pairs	22
Pearson r	0.7457
95% confidence interval	0.4726 to 0.8881
P value (two-tailed)	< 0.0001
P value summary	****
Is the correlation significant? (alpha=0.05)	Yes
R square	0.5560

Supplement Fig. 6. Correlation between myofibroblast population and lung weight in BLM treated rats. Total twenty-two rats were treated with BLM (same regimen as Fig. 1) and the lung tissues were collected for myofibroblast isolation following lung weight measurement at different time-points after BLM induction (Day 7, 14, 21 and 28).

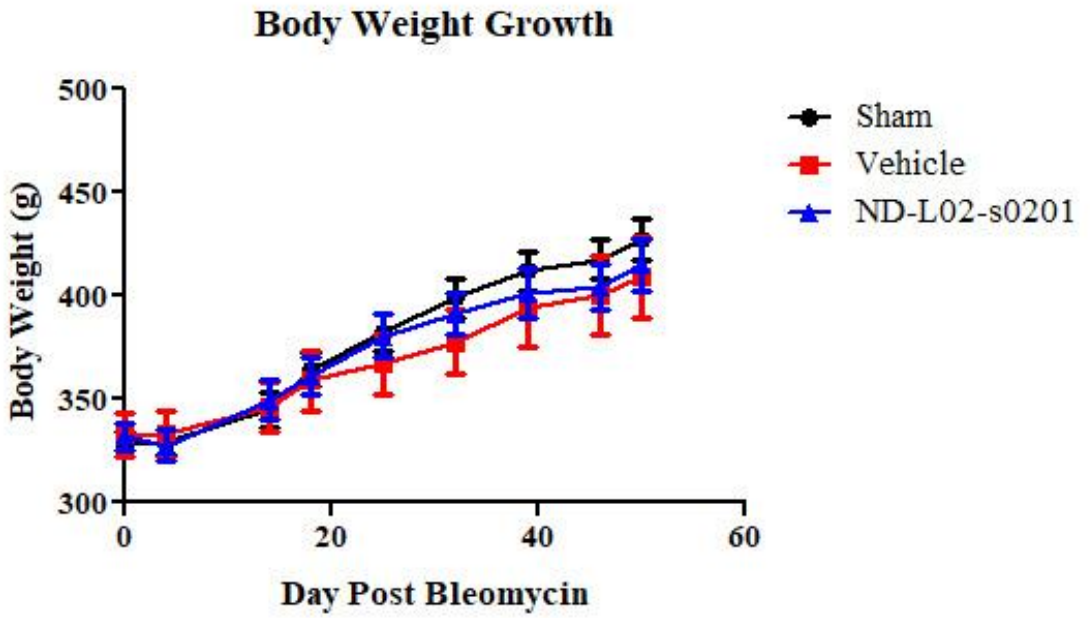

Supplement Fig. 7. Animal body weight growth during running endurance evaluation following BLM induction in rat chronic model of lung fibrosis. The test condition was described as in Fig. 5.

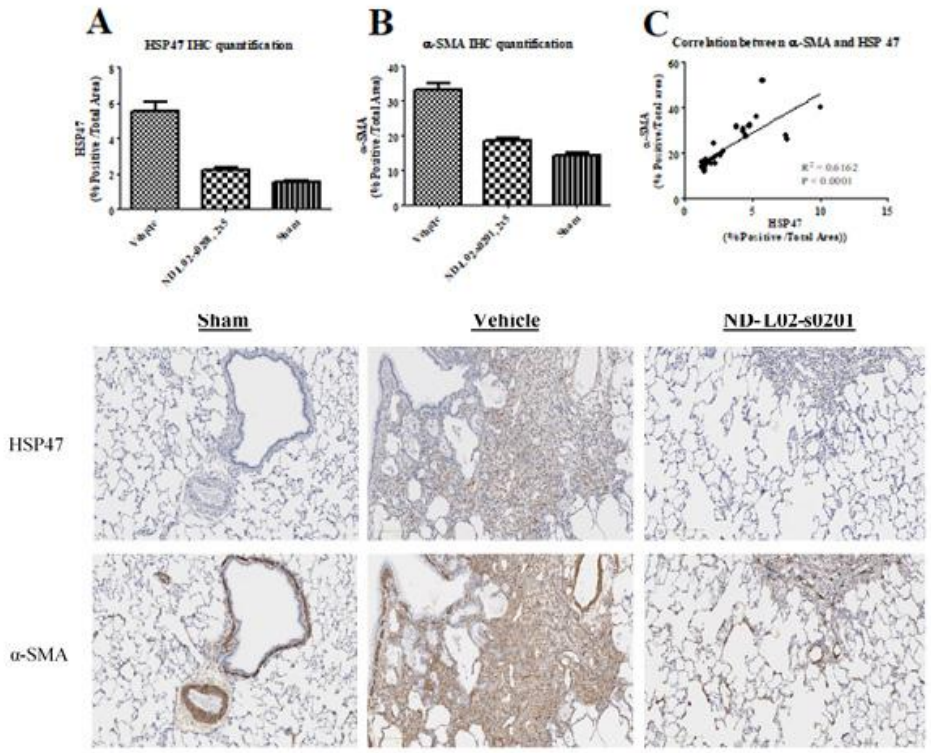

Supplement Fig. 8. Image quantification analyses of anti-HSP47 or α-SMA IHC staining from the sequential sections of BLM treated rat lung tissue. Male Sprague-Dawley rats were treated with BLM eight times at 3 mg/kg (Day 0, 14) and 1 mg/kg (Day 1 to Day 6) to induce chronic lung damage. ND-L02-s0201 was dosed IV at 2 mg/kg, QW x five weeks Day 18 following initial BLM induction. (A) Image quantification of HSP47 IHC stain, (B) Image quantification of α-SMA IHC stain and (C) Correlation analysis of IHC stains between HSP47 and α-SMA. Representative images of anti HSP47 (top panel) or α-SMA (low panel) IHC stain of sequential sections from BLM rat lung tissue (10 x).

Supplement Tab 1. Fibrosis RT^2 Profiler PCR Arrays (Qiagen) on eighty-four genes of rat lung tissues. Relative gene expression levels were expressed as fold-change following either BLM induction alone (n = 6) or BLM + ND-L02-s0201 (1.5 mg/kg/week, four weeks) treatment (n = 6) related to Sham Group (n = 4). Fold-Changes were calculated using 2^ (-ΔΔCt CT) formula.

Gene Symbol	Description	Gene Fold-Changes	
		BLM alone	BLM + ND-L02-s0201
Acta2	Smooth muscle alpha-actin	1.536	1.1159
Agt[*]	Angiotensinogen (serpin peptidase inhibitor, clade A, member 8)	3.147	5.1047
Akt1	V-akt murine thymoma viral oncogene homolog 1	1.1504	-1.4265
Bcl2[ξ]	B-cell CLL/lymphoma 2	1.6407	-1.2021
Bmp7	Bone morphogenetic protein 7	-1.9549	-1.8196
Cav1[ξ]	Caveolin 1, caveolae protein	-1.415	1.3392
Ccl11[ξ]	Chemokine (C-C motif) ligand 11	-1.923	1.3112
Ccl12	Chemokine (C-C motif) ligand 12	1.8419	1.1433
Ccl3[ξ]	Chemokine (C-C motif) ligand 3	1.2206	-1.0601
Ccr2[ξ]	Chemokine (C-C motif) receptor 2	3.4077	1.6814
Cebpb[ξ]	CCAAT/enhancer binding protein (C/EBP), beta	1.0668	-1.0679
Col1a2[*, ξ]	Collagen, type I, alpha 2	3.592	-1.0581
Col3a1[*, ξ]	Collagen, type III, alpha 1	3.4519	1.136
Ctgf[*, ξ]	Connective tissue growth factor	2.143	-1.4466
Cxcr4	Chemokine (C-X-C motif) receptor 4	1.5641	1.1641
Dcn[*]	Decorin	-2.8133	-1.7326
Edn1[*]	Endothelin 1	2.4282	1.0891
Egf[*]	Epidermal growth factor	-2.1586	-1.9671

Eng	Endoglin	1.0173	-1.78
Faslg	Fas ligand (TNF superfamily, member 6)	-1.5083	-2.844
Grem1[*, ξ]	Gremlin 1, cysteine knot superfamily, homolog (Xenopus laevis)	6.2729	-1.7664
Hgf	Hepatocyte growth factor	1.4619	-1.2472
Ifng[ξ]	Interferon gamma	-1.432	1.1745
Il10	Interleukin 10	-1.1964	-1.2874
Il13[*]	Interleukin 13	-3.7558	-3.9919
Il13ra2[*]	Interleukin 13 receptor, alpha 2	-4.1883	-4.4439
Il1a[ξ]	Interleukin 1 alpha	1.2016	-1.4653
Il1b[ξ]	Interleukin 1 beta	1.1479	-1.0713
Il4[*]	Interleukin 4	-2.5329	-2.5989
Il5[ξ]	Interleukin 5	-1.8821	1.7433
Ilk	Integrin-linked kinase	1.5692	1.3277
Inhbe[*]	Inhibin beta E	-4.1883	-4.4439
Itga1	Integrin, alpha 1	-1.5497	-3.2797
Itga2[*, ξ]	Integrin, alpha 2	2.3786	-1.3272
Itga3	Integrin, alpha 3	1.7594	1.1128
Itgav[ξ]	Integrin, alpha V	1.821	-1.3337
Itgb1[*, ξ]	Integrin, beta 1	5.0062	2.7398
Itgb3	Integrin, beta 3	-1.0391	-1.2524
Itgb5	Integrin, beta 5	-1.0231	-2.1338
Itgb6	Integrin, beta 6	1.1853	-1.3146
Itgb8	Integrin, beta 8	1.7626	1.0147
Jun[*]	Jun oncogene	2.005	1.2567
Lox[*, ξ]	Lysyl oxidase	2.9497	-1.0426
Ltbp1[ξ]	Latent transforming growth factor beta binding protein 1	1.5587	-1.0862
Mmp13[*]	Matrix metallopeptidase 13	-3.1857	-4.0202
Mmp14[*]	Matrix metallopeptidase 14 (membrane-inserted)	2.6236	1.1419
Mmp1[*]	Matrix metallopeptidase 1a (interstitial collagenase)	-5.2566	-5.5774
Mmp2[*, ξ]	Matrix metallopeptidase 2	3.567	1.0756

Mmp3[*]	Matrix metallopeptidase 3	-2.7467	-4.4439
Mmp8	Matrix metallopeptidase 8	-1.0371	-1.0956
Mmp9	Matrix metallopeptidase 9	1.0432	1.0773
Myc	Myelocytomatosis oncogene	1.8077	1.7728
Nfkb1	Nuclear factor of kappa light polypeptide gene enhancer in B-cells 1	1.5246	-1.0677
Pdgfa	Platelet-derived growth factor alpha polypeptide	1.0067	-1.0273
Pdgfb[ξ]	Platelet-derived growth factor beta polypeptide (simian sarcoma viral (v-sis) oncogene homolog)	1.1111	-2.1585
Plat[*, ξ]	Plasminogen activator, tissue	5.6391	3.3442
Plau[*, ξ]	Plasminogen activator, urokinase	2.2371	-1.0942
Plg[*, ξ]	Plasminogen	8.0086	4.5203
Serpina1	Serpin peptidase inhibitor, clade A (alpha-1 antiproteinase, antitrypsin), member 1	1.6863	2.2534
Serpine1[*, ξ]	Serpin peptidase inhibitor, clade E (nexin, plasminogen activator inhibitor type 1), member 1	12.3588	2.8291
Serpinh1[*] (HSP47)	Serine (or cysteine) peptidase inhibitor, clade H, member 1	2.2791	1.2243
Smad2	SMAD family member 2	-1.1286	-2.1036
Smad3[ξ]	SMAD family member 3	1.0536	-1.599
Smad4	SMAD family member 4	-1.9082	-1.7313
Smad6[ξ]	SMAD family member 6	1.193	-1.0832
Smad7	SMAD family member 7	-1.1216	-1.9593
Snai1[*, ξ]	Snail homolog 1 (Drosophila)	9.8467	6.0475
Sp1[ξ]	Sp1 transcription factor	1.4969	-1.1213
Stat1[ξ]	Signal transducer and activator of transcription 1	1.0245	-1.2164
Stat6	Signal transducer and activator of transcription 6	1.292	1.1881
Tgfb1[ξ]	Transforming growth factor, beta 1	1.1571	-1.2068
Tgfb2[ξ]	Transforming growth factor, beta 2	1.3323	-1.6495

Tgfb3[ξ]	Transforming growth factor, beta 3	1.278	-2.4358
Tgfbr1[ξ]	Transforming growth factor, beta receptor 1	1.6867	-1.6032
Tgfbr2[ξ]	Transforming growth factor, beta receptor II	1.9345	-1.0495
Tgif1[ξ]	TGFB-induced factor homeobox 1	1.0034	-1.4144
Thbs1[ξ]	Thrombospondin 1	2.1517	-1.7516
Thbs2[*, ξ]	Thrombospondin 2	22.7212	1.7471
Timp1[*]	TIMP metallopeptidase inhibitor 1	2.4288	1.274
Timp2[ξ]	TIMP metallopeptidase inhibitor 2	1.053	-1.1596
Timp3	TIMP metallopeptidase inhibitor 3	-1.033	-1.5895
Timp4[ξ]	Tissue inhibitor of metalloproteinase 4	-1.0028	1.6266
Tnf	Tumor necrosis factor (TNF superfamily, member 2)	-1.2244	-1.6372
Vegfa	Vascular endothelial growth factor A	-1.8622	-2.7792

[*] Fold-change cut-off > 2 following BLM induction *v.s.* Sham Group.

[ξ] Fold-change cut-off > 1.5 following BLM + ND-L02-s0201 *v.s.* BLM induction alone Group.